Int J Adv Manuf Technol
DOI 10.1007/s00170-011-3375-6

ORIGINAL ARTICLE

Modeling and vibration mode analysis of a ball screw drive

Diego A. Vicente · Rogelio L. Hecker · Fernando J. Villegas · Gustavo M. Flores

Received: 30 December 2010 / Accepted: 1 May 2011

Abstract Positioning systems for machine tools are generally driven by ball screws due to their high stiffness and low sensitivity to external perturbations. However, as modern machine tools increase their velocity and acceleration of positioning, the resonant modes of these systems could be excited degrading the trajectory tracking accuracy. Therefore, a dynamic model including the vibration modes is required for machine design as well as for controller selection and tuning. This work presents a high-frequency dynamic model of a ball screw drive. The analytical formulation follows a comprehensive approach, where the screw is modeled as a continuous subsystem, using Ritz series approximation to obtain an approximate *N*-degree-of-freedom model. Based on this model, the axial and angular components of each mode function are studied for different transmission ratios to determine the degree of coupling between them. After that, the frequency variation of each mode was studied for different carriage positions and different moving masses. Finally, an analysis of these results applied to controller design and parameter estimation is also presented.

Keywords Feed drive · Ball screw · Vibration modes · Machine tools

1 Introduction

High-performance feed drives are required in modern machine tools to achieve high-quality parts and cycle time reduction [1]. Ball screw feed drives are widely used for positioning due to their relative low cost and low sensitivity to external forces and inertia variations, compared to linear motors. However, the high-frequency dynamics of a ball screw must be considered for high accelerations, where the system modes can be excited degrading the position accuracy. This is the case of high speed machining, where the feed between the cutting tool and the workpiece increases proportionally to the increased spindle speed [2]. This represents a problem, particularly in machining parts that require short and repetitive movements resulting in demanding acceleration profiles. Therefore, traditional models must be augmented with higher-order dynamics to assist the controller design.

Since low-order models are preferable for controller design and tuning, a model with 2 degrees of freedom can be used, which is able to capture the rigid body mode and the first vibration mode with some degree of accuracy [3–5]. This kind of model is useful when the position loop is closed with the direct carriage position. However, higher resonant frequencies become important when closing the loop with rotary sensors at the motor position [2, 6].

D. A. Vicente · G. M. Flores
Universidad Nacional de La Pampa,
General Pico 6360, La Pampa, Argentina

R. L. Hecker (✉)
Universidad Nacional de La Pampa—CONICET,
Calle 110 Nro. 390, General Pico 6360,
La Pampa, Argentina
e-mail: hecker@ing.unlpam.edu.ar

F. J. Villegas
CONICET, General Pico 6360,
La Pampa, Argentina

Published online: 24 May 2011

On the other hand, modern tendencies of virtual machine design require more accurate models to predict the system dynamics, in order to anticipate its interaction with the machining process [7]. In this sense, an accurate model for a positioning system must include high-frequency vibration modes in order to capture the interaction of design parameters and operating conditions with respect to dynamic response.

A comprehensive model was presented by Varanasi [3], where the screw was considered as a distributed parameter system in which the axial and torsional deformation fields were simplified to vary linearly with the axial coordinate of the screw. However, the model includes only two generalized coordinates, making it suitable for specific control purposes but not allowing higher-frequency analysis.

Smith [2] modeled the ball screw with finite element method (FEM) beam formulation to draw conclusions about the behavior of the system in each mode and to predict the vibration frequencies. Alternatively, Erkorkmaz and Kamalzadeh [6] measured screw torsional deformations at particular locations to experimentally verify the mode shapes prediction from a FEM. The authors of both works agree that the first mode is mainly axial whereas the second and third are mainly torsional. However, these conclusions are drawn for their particular systems under a fixed operating condition.

Chen et al. [8] used a mechanical model of a ball screw to study the contouring error due to the compliance effect. The model has 5 degrees of freedom, and it predicts the rigid rotation, axial, and torsional vibration of the ball screw and axial and rotational vibration of the whole table. Although the model is suitable for the particular analysis done by the authors, the formulation uses only lumped parameters, and it does not predict the screw deformation in each mode. In addition, the table rotation becomes important only when the machining area is at a high vertical distance with respect to the table base.

Models accounting for lateral deformation, in addition to the axial and torsional, were presented by Zaeh et al. [9] and Okwudire and Altintas [10]. The main difference between both models is that the latter is able to capture the coupling between axial–torsional and lateral vibrations whereas the former only captures the coupling between the axial and torsional. For both models, a detailed screw–nut interface is proposed, which implies that a significant number of parameters must be known.

From this review, it can be seen a need for a model with capabilities for virtual machine design as well as for controller selection and tuning. The model must capture the dynamics of the first resonant modes with parameters that are generally available from component manufacturers or easily estimated. Particularly, it is important for modern control strategies to study the degree of coupling between the main modes as a function of system parameters and operating conditions. In this way, this work proposes a model based on a combination of concentrated and distributed parameters. After that, the mode shapes are obtained and analyzed for two typical transmission ratios, and the variations of the mode frequencies are studied for different carriage positions and different moving masses. Finally, the results are analyzed drawing conclusions about the system behavior, which can be helpful as a first guideline for control process design and system identification.

2 Servomechanism model

The most common feed drive for precision positioning consists of a ball screw, assembled to the machine base by rotary bearings, which is driven by an electric servomotor through a flexible coupling, as Fig. 1 shows. The ball nut is attached to the carriage that is constrained to move axially on linear bearings and guideways.

The schematic model considered here is presented in Fig. 2, in which the screw is considered as a continuous system, whereas the remaining elements are assumed in the lumped form. In these conditions, the screw can be considered as a straight bar with three fundamental types of deformations: axial deformation, by traction or compression; angular deformation, by torsion; and flexural deformation. Flexure is discarded, assuming the screw is suitably mounted in the servomechanism and then minimizing buckling due to non-concentric forces produced by misalignments.

In this way, the continuous deformation can be represented by an axial displacement using a field function $u(x, t)$ and by an angular displacement using $\theta(x, t)$. This continuous portion is characterized by mass density ρ, cross section A, moment of inertia J_t, length L, modulus of Young E, modulus of Poisson G, and screw lead l (also cited as transmission ratio).

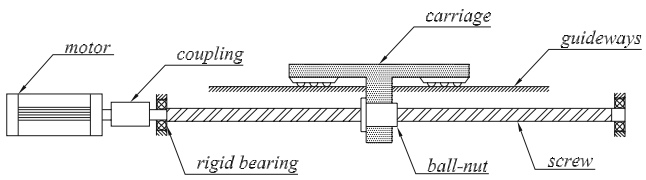

Fig. 1 Ball screw feed system

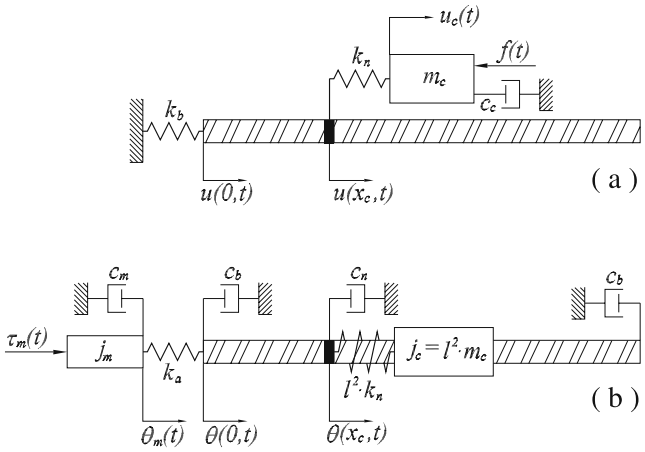

Fig. 2 Schematic of the axial (**a**) and rotational (**b**) decoupled models

The elements assumed in the lumped form are the rotor of the electric motor with moment of inertia J_m, the flexible coupling with moment of inertia J_a and stiffness k_a, the rigid bearing with stiffness k_b, the nut with stiffness k_n, and the carriage with mass m_c.

2.1 Selection of the basis functions

The deformation in a continuous general system can be represented by a displacement field $u(x,t)$ that is a function of time and spatial coordinates. The Ritz series method [11], also known as the method of assumed modes, uses a series expansion to describe the displacement field as follows:

$$u(x,t) = \sum_{j=1}^{N} \psi_j(x) q_j(t) \tag{1}$$

where $\psi_j(x)$, known as basis functions, represent the displacement field as a function of the x coordinate and the coefficients $q_j(t)$ represent the instantaneous contribution of $\psi_j(x)$ over the displacement field.

The basis functions must fulfill certain conditions to obtain a valid formulation of the Ritz series. All basis functions must be continuous, linearly independent, and must satisfy the geometric boundary conditions [11]. In this way, a suitable axial field equation can be constructed using cosine basis functions as follows:

$$u(x,t) = \sum_{j_u=1}^{N_u} \cos\left(\alpha \frac{x}{L}\right) q_{j_u}(t) \tag{2}$$

where $\alpha = (j_u - 1)\pi$. The first term in the series (with $j_u = 1$) is the unitary function that represents the rigid body motion which is kinematically admissible for this system. This is because the screw is attached to the base by the bearing, which is modeled as a lumped spring, as Fig. 2a shows. Although the axial rigid body motion would not actually occur, it is advisable to introduce a unitary function to account for stiffness differences between the screw and the rigid bearing [11].

It is more obvious that the screw has a rigid body motion for the angular displacement; then, the displacement field to describe rotation in the screw can be represented by

$$\theta(x,t) = \sum_{j_\theta=1}^{N_\theta} \cos\left(\alpha \frac{x}{L}\right) q_{j_\theta}(t) \tag{3}$$

where $\alpha = (j_\theta - 1)\pi$. The number of terms N_u and N_θ can be selected by studying the convergence of the model solutions.

2.2 Equations of motion based on energy and work formulation

A convenient way to find the equations of motion of a multibody system is using the energy and work formulation, which is more efficient and reliable than the Newton–Euler formulation based on momentum considerations.

Using the defined variables, the kinetic energy can be computed as follows:

$$T = \frac{1}{2} m_\mathrm{c} \dot{u}_\mathrm{c}(t)^2 + \frac{1}{2} J_\mathrm{m} \dot{\theta}_\mathrm{m}(t)^2 + \frac{1}{2} J_\mathrm{a} \left(\frac{\dot{\theta}_\mathrm{m}(t) + \dot{\theta}(0,t)}{2}\right)^2 + \frac{1}{2}\rho J_t \int_0^L \dot{\theta}(x,t)^2 \mathrm{d}x + \frac{1}{2}\rho A \int_0^L \dot{u}(x,t)^2 \mathrm{d}x \tag{4}$$

where the first and second terms represent the contributions from the mass of the carriage and the inertia of the rotor, respectively. The third term is the energy from the flexible coupling, for which an average speed between the angular velocity of the rotor and the angular velocity of the screw in $x = 0$ was considered. The fourth and fifth terms represent the kinetic energy from the distributed rotary inertia and the distributed linear inertia of the screw, respectively.

The potential energy stored in the elastic parts of the system can be computed according to

$$V = \frac{1}{2} k_\mathrm{b} u(0,t)^2 + \frac{1}{2} k_\mathrm{a} \left[\theta_\mathrm{m}(t) + \theta(0,t)\right]^2 + \frac{1}{2} k_\mathrm{n} \delta_\mathrm{n}^2 + \frac{1}{2} J_t G \int_0^L \left(\frac{\mathrm{d}\theta(x,t)}{\mathrm{d}x}\right)^2 \mathrm{d}x + \frac{1}{2} EA \int_0^L \left(\frac{\mathrm{d}u(x,t)}{\mathrm{d}x}\right)^2 \mathrm{d}x \tag{5}$$

where the first and second terms correspond to the potential energy in the rigid bearing and flexible coupling,

respectively. Similarly, the third term corresponds to the potential energy stored in the ball nut, where δ_n is the axial deformation in the nut. Although the elastic deformation in the screw–nut interface produced by the normal contact force has axial and radial components [12], only the axial component influences the axial displacement field.

Therefore, the interface axial deformation can be expressed as

$$\delta_n = u_c(t) - \big(u(x_c, t) + \theta(x_c, t)l\big) \tag{6}$$

that denotes the difference between the absolute position of the carriage, $u_c(t)$, and the absolute position of the screw at the interface-point coordinate x_c. It is important to notice that Eq. 6 involves both axial and torsional displacements, showing a coupling between them, a fact that forbids each field to be treated separately. Finally, the fourth and fifth terms of Eq. 5 represent the potential energy stored in the continuous portion of the system, the screw, by torsional and axial displacements.

The net power input to the system results in

$$P_{in} = \tau_m \dot{\theta}_m(t) - \tau_f \dot{\theta}(x_c, t) - f_c \dot{u}_c(t) \tag{7}$$

where the first term is the power input from the motor, the second term is the Coulomb friction dissipation in the ball nut due to the friction torque τ_f, and the third term represents the power required to move the carriage at the velocity $\dot{u}_c$ against a disturbance force f_c. Note that f_c is a general variable to account for external forces acting on the carriage, which can include machining forces and Coulomb friction forces in guideways.

Finally, the power dissipation in the system due to viscous friction can be expressed as follows:

$$\begin{aligned} P_{dis} = & \int_0^L \gamma EA \left(\frac{\mathrm{d}u(x,t)}{\mathrm{d}x}\right)^2 \mathrm{d}x \\ & + \int_0^L \gamma GJ_t \left(\frac{\mathrm{d}\theta(x,t)}{\mathrm{d}x}\right)^2 \mathrm{d}x + c_m \dot{\theta}_m(t)^2 \\ & + c_b \dot{\theta}(0,t)^2 + c_n \dot{\theta}(x_n,t)^2 + c_c \dot{u}_c(t)^2 \end{aligned} \tag{8}$$

The first two terms represent the power dissipation due to the viscoelastic behavior of the continuous portion, where γ is the structural damping loss factor. The other four terms represent the power dissipation in rotor bearings, screw supporting bearings, ball nut, and guideways, respectively. Therefore, the coefficients c_m, c_b, c_n, and c_c are the viscous friction coefficients of these elements, as Fig. 2 shows.

Now the expressions of T, V, P_{in}, and P_{dis} are combined with the Ritz series to formulate the Lagrange procedure in order to find the equations of motion. Alternatively, the power balance methodology can be used in this particular case, giving the same results as those obtained by Lagrange formulation but with an easier derivation [11]. In any case, the equations of motion can be expressed as

$$[M][\ddot{q}] + [C][\dot{q}] + [K][q] = [Q] \tag{9}$$

where M, C, and K are the inertia, damping, and stiffness matrices, respectively. The vector Q includes the generalized forces and q are the generalized coordinates.

As Fig. 2 shows, in addition to the generalized coordinates from the continuous portion, there are two additional generalized coordinates, one to describe the carriage position $u_c(t)$ and another to describe the rotor angular position $\theta_m(t)$. Therefore, the total system order is $N = N_U + N_\Theta$, with $N_U = N_u + 1$ and $N_\Theta = N_\theta + 1$.

3 Modal formulation

The solution of the eigenvalue problem $[[K]-\omega_j{}^2[M]]\{\phi_j\}=[0]$ related to Eq. 9 gives N eigensolutions, each one featuring a natural frequency ω_j and a normal mode $\{\phi_j\}$. Applying the modal transformation $\{q\} = [\phi]\{\eta\}$, the displacement field presented in Eq. 1 can be expressed as

$$u(x,t) = [\psi][\phi]\eta = [\Psi]\eta \tag{10}$$

where $[\psi]$ is a row composed of the basis functions $[\psi] = [\psi_1 .... \psi_N]$ and $[\Psi]$ is a row composed of the functions $[\Psi] = [\psi]\{\phi_j\}$, known as mode functions. As the elements of the mode vector $\{\phi_j\}$ give the proportions between the various generalized coordinates, the mode function Ψ_j gives the deformation proportions as a function of the x coordinate, in the jth mode.

On the other hand, the η_j represents the mode contribution to the displacement field. However, this is not included in the following analysis because it is intended to draw conclusions from the general system regardless of excitation type and initial conditions.

To compute the axial and angular components of the mode functions, it is necessary to distinguish, in each mode vector $\{\phi_j\}$, the elements corresponding to each generalized coordinate. In this sense, if the generalized coordinates vector q has the following arrangement:

$$\{q\} = \left\{q_{u_1} ... q_{u_{N_u}}\ q_{\theta_1} ... q_{\theta_{N_\theta}}\ u_c\ \theta_m\right\}^T \tag{11}$$

each mode vector $\{\phi_j\}$ can be written as

$$\{\phi_j\} = \left\{\phi_{u_1} \ldots \phi_{u_{N_u}}\ \phi_{\theta_1} \ldots \phi_{\theta_{N_\theta}}\ \phi_{u_c}\ \phi_{\theta_m}\right\}^T \tag{12}$$

Therefore, the first N_u elements of $\{\phi_j\}$ are associated with the axial displacements and the following N_θ elements of $\{\phi_j\}$ are associated with the angular displacements, whereas the last two elements of $\{\phi_j\}$, ϕ_{u_c}, and ϕ_{θ_m} are the elements describing the carriage displacement and the angular displacement of the motor rotor, respectively. In this way, the axial component of the jth mode function can be constructed from the basis functions used to describe the axial field and the first N_u elements of $\{\phi_j\}$ as follows:

$$\Psi_{u_j}(x) = \left[\psi_{u_1}(x) \ldots \psi_{u_{N_u}}(x)\right]\left\{\phi_{u_1} \ldots \phi_{u_{N_u}}\right\}^T \tag{13}$$

Similarly, the angular component of the jth mode function results in

$$\Psi_{\theta_j}(x) = \left[\psi_{\theta_1}(x) \ldots \psi_{\theta_{N_\theta}}(x)\right]\left\{\phi_{\theta_1} \ldots \phi_{\theta_{N_\theta}}\right\}^T \tag{14}$$

In an effort to validate the model, the calculated natural frequencies ω_j were compared to the measured ones from other authors. For example, Varanasi [13] measured only the first vibration mode at 349 Hz. The model proposed here tuned with the system parameters presented by Varanasi [13] predicts the first mode at 338 Hz, which results in a very good agreement with the measured one. Similarly, the first three mode frequencies for another system were measured by Smith [2] at 65, 512, and 1,045 Hz. The model tuned with the system parameters presented by Smith [2] predicts these modes at 65, 760, and 949 Hz, respectively, which are in a reasonable agreement as well.

4 Analysis of the mode functions for different transmission ratios

The mode functions were obtained according to Eqs. 13 and 14 in which the mode vectors correspond to the system solution with the physical parameters in Table 1, the particular carriage position $x_c = 0.5$ L, and a total moving mass of $m_c = 30$ kg. The number of terms in the Ritz series were $N_u = N_\theta = 4$ obtaining a suitable compromise between model complexity and estimation error [14]. From Eq. 6, it can be seen that the transmission ratio has a direct influence on the degree of coupling between the axial and torsional deformation fields. Therefore, two particular values of transmission ratio (screw lead) are selected for the following study.

Figure 3 shows the axial and angular components of the mode functions for the first four modes for a transmission ratio of 10 mm/rev. Also, in Fig. 3a, the displacement of the carriage was described in each mode as a point value $\phi_{u_c j}$ plotted at $x = x_c$. Similarly, in Fig. 3b, the displacement of the motor rotor was described by $\phi_{\theta_{m j}}$ plotted at $x_m = -0.2$ L. Note that the zero coordinate is located at the rigid bearing; therefore, the middle of the motor is located at negative coordinate values.

Table 1 Parameter values used in the model

ρ	7,850	(kg/m^3)
E	2.06×10^{11}	(N/m^2)
G	8.1×10^{10}	(N/m^2)
A	4.22×10^{-4}	(m^2)
J_t	2.8×10^{-8}	(m^4)
L	0.743	(m)
J_a	3.8×10^{-4}	(kg m^2)
J_m	2.6×10^{-4}	(kg m^2)
k_n	4.3×10^8	(N/m)
k_b	4.5×10^8	(N/m)
k_a	5,200	(Nm/rad)

The rigid body mode is represented by Ψ_{u0} and $\Psi_{\theta 0}$, where the screw is not showing any kind of deformation. In this case, the carriage motion $\phi_{u_c 0}$ is exactly l times the angular motion $\Psi_{\theta 0}$. Similar results can be observed in Fig. 4 for a transmission ratio of 32 mm/rev.

The next analysis attempts to visualize the character of each mode, basically the degree of axial or torsional predominance. This analysis is based not only on the mode shapes but also on the agreement between the natural frequencies from the coupled system respect to the pure axial and torsional natural frequencies. The latter are obtained from the uncoupled axial and torsional models derived from the general model assuming components with infinite torsional and axial stiffness, respectively [15], according to Fig. 2 and the derived equations in Section 2.2.

Table 2 compares the natural frequencies for the coupled and decoupled solutions for a transmission ratio of 10 mm/rev. The classification, either as torsional or axial, of the modes from the coupled model is done based on the best agreement between the frequencies of both models. The last column shows the error in the natural frequency values from decoupled system solutions; in this sense, a greater error means greater axial–torsional coupling. Similarly, Table 3 shows the results for a screw lead of 32 mm/rev.

4.1 Mode analysis for a low transmission ratio

Figure 3 shows the first vibrating mode, where the axial component amplitude Ψ_{u1} has the greatest values compared to their homologs, whereas the angular $\Psi_{\theta 1}$ has

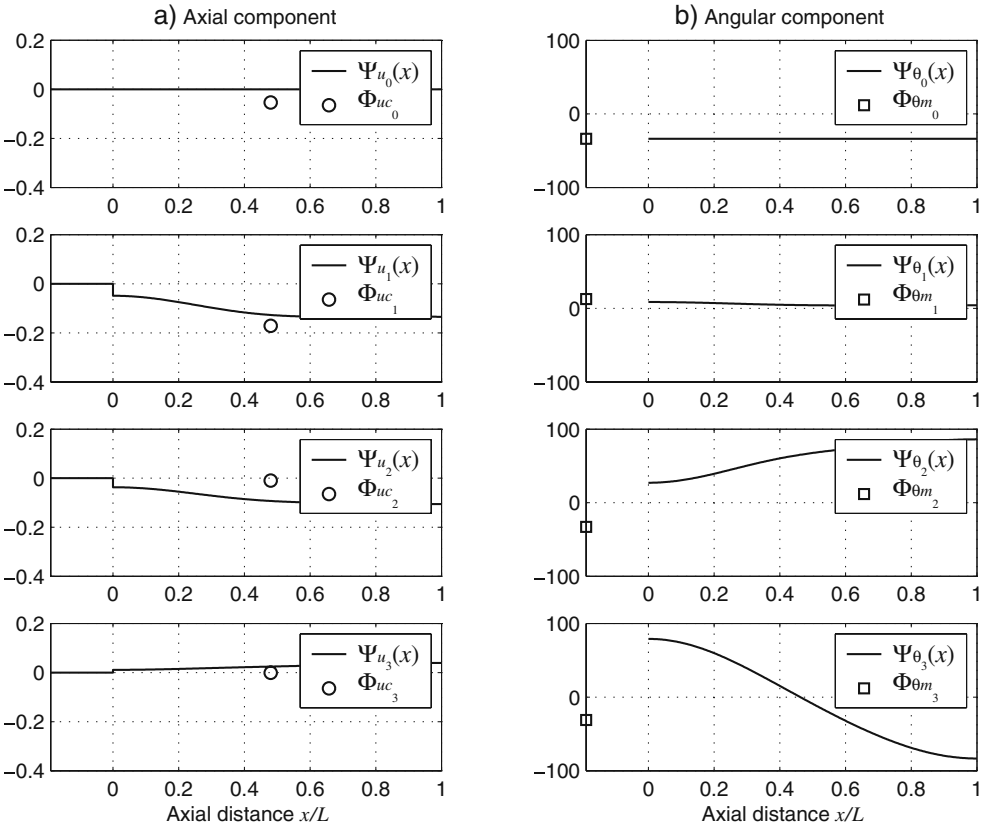

Fig. 3 Axial and angular components of the mode functions for $l = 10$ mm/rev

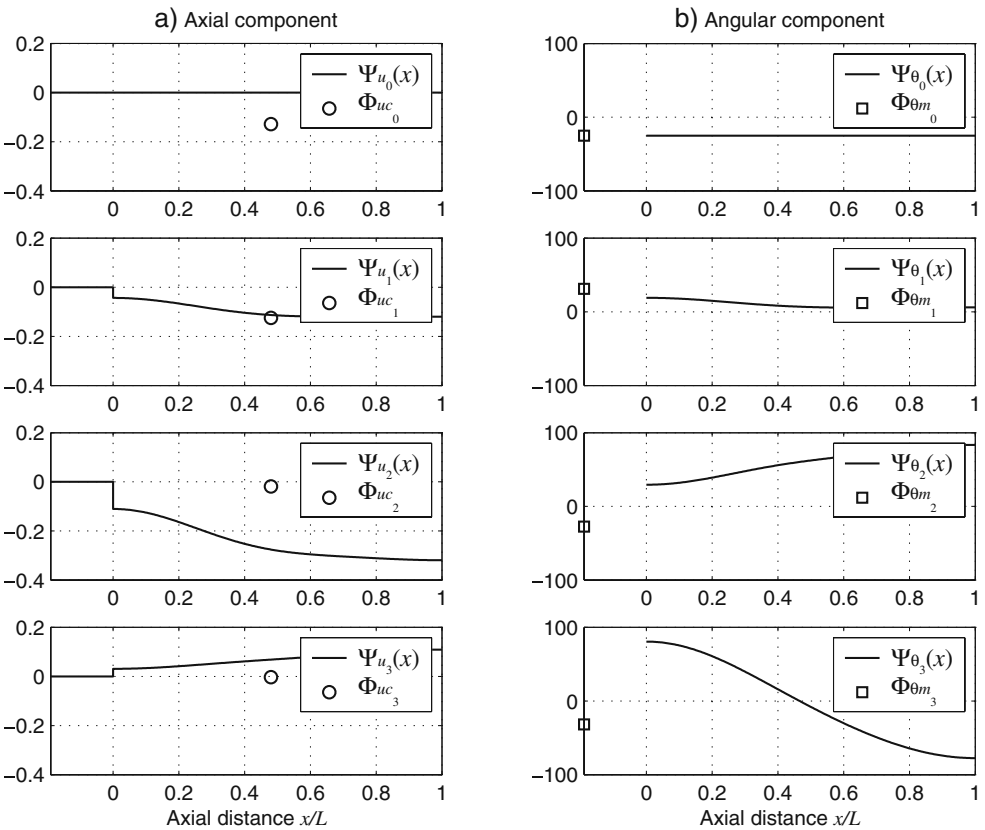

Fig. 4 Axial and angular components of the mode functions for $l = 32$ mm/rev

Table 2 Frequencies comparison for $l = 10$ mm/rev and for $N_u = N_\theta = 3$

Mode	Coupled (rad/s)	Axial decoupled (rad/s)	Torsional decoupled (rad/s)	Error (%)
ω_0	0	–	0	0.00
ω_1	2,045	2,000	–	2.20
ω_2	5,924	–	5,054	14.69
ω_3	12,679	–	12,647	0.25

the smallest one. In addition, the displacement of the carriage ϕ_{u_c1} has the largest value, which is consistent with [2], in which the first vibration mode was described as an axial mode with a large carriage displacement. This can also be seen by the very good match of ω_1 between the coupled system and the axial decoupled subsystem as is shown in Table 2.

In the second mode, the amplitude of the angular component increases considerably as Fig. 3 shows, whereas the axial decreases and the axial displacement of the carriage is substantially lower. Nevertheless, the axial mode function amplitude keeps a significant value. It means that the axial and angular deformations could both be important. However, the frequency analysis in Table 2 shows that there is a reasonable match between the frequency of the coupled system and the frequency from the torsional subsystem at ω_2. Therefore, this is a predominantly torsional mode with some degree of axial coupling.

Finally, the angular component in the third mode shows the largest amplitude, whereas the axial and the carriage displacements are very small. Therefore, this mode seems to be predominantly torsional, and this is confirmed by the good match that ω_3 shows in Table 2.

4.2 Mode analysis for a high transmission ratio

Figure 4 shows the mode shapes for a transmission ratio of $l = 32$ mm/rev. It can be observed that the axial component of the first mode slightly decreases, whereas the torsional component slightly increases, both respect to a transmission ratio of $l = 10$ mm/rev. On the other hand, Table 3 shows an error of about 10% when ω_1 is compared with the axial uncoupled frequency. Therefore, it is concluded that this mode remains with an axial predominance with a slight degree of torsional coupling. The axial component of the second vibration mode shows the largest amplitude among the other axial components. Furthermore, the frequency match with respect to an uncoupled torsional mode shows about 50% of error at ω_2; therefore, this mode shows a high degree of coupling with no clear predominant type of deformation.

Finally, the third mode remains with a torsional predominance as can be seen from the mode shape components and the frequency match at ω_3.

Table 3 Frequencies comparison for $l = 32$ mm/rev and for $N_u = N_\theta = 3$

Mode	Coupled (rad/s)	Axial decoupled (rad/s)	Torsional decoupled (rad/s)	Error (%)
ω_0	0	–	0	0.00
ω_1	2,236	2,000	–	10.55
ω_2	6,595	–	3,363	49.01
ω_3	12,657	–	12,548	0.86

5 Mode frequency variation for different operating conditions

The mode shapes and their frequencies are sensitive not only to design parameters, as was shown for different transmission ratios, but also to operation conditions, like carriage position and total moving mass. The results presented in the previous sections are for a carriage position of $x_c = 0.5$ L and a total mass of $m_c = 30$ kg. Following, the natural frequencies were studied for different carriage positions, different moving masses, and the combination of them, all for the two proposed transmission ratios. In each case, the natural frequency deviation for each mode was computed according to

$$\Delta\omega = \frac{\omega_{\max} - \omega_{\min}}{\omega_{\min}} 100 \tag{15}$$

where $\omega_{\max}$ and $\omega_{\min}$ are, respectively, the maximum and minimum values of each natural frequency, for the three variable conditions studied, defined as follows:

Variable position: carriage positions between 0.1 and 0.9 L and a fixed load mass $m_c = 30$ kg.
Variable mass: load mass variations between 30 and 150 kg with a fixed carriage position $x_c = 0.5$ L.
Variable position and mass: variations for a load mass between 30 and 150 kg evaluated at each carriage position of 0.1 and 0.9 L.

Table 4 First natural frequency variation for different operating conditions

Operation conditions	$l = 10$ mm/rev (%)	$l = 32$ mm/rev (%)
Variable position	60	70
Variable mass	98	28
Variable position and mass	216	119

Table 5 Second natural frequency variation for different operating conditions

Operation conditions	$l = 10$ mm/rev (%)	$l = 32$ mm/rev (%)
Variable position	0.8	5.6
Variable mass	0.1	0.4
Variable position and mass	1.0	6.5

In this way, the rows of Table 4 show the relative deviation of the first natural frequency for the three operation conditions, evaluated at the two transmission ratios. Similarly, Tables 5 and 6 show the results for the second and third vibration modes, respectively.

According to results in Table 4, the first mode shows to be very sensitive to the carriage position for both transmission ratios. Also it is very sensitive with respect to mass changes for low screw lead but much less sensitive when the screw lead increases. This last behavior can be explained using conclusions from the degree of coupling analyzed in the previous section. For low axial–torsional coupling, as is the case for low transmission ratios, this mode is strongly axial and behaves like a spring mass system; therefore, it is very sensitive to mass changes. However, as the screw lead increases, the axial component is more coupled with the torsional component, where the latter is less sensitive to mass changes due to the reduction imposed by the transmission. As can be expected, this mode presents high sensitivity to the combined effects of load mass and carriage position variations.

On the other hand, the second mode in general presents low variations with respect to mass and position changes, as Table 5 shows, due to its torsional predominance. Particularly, the frequency variation increases up to 5.6% for high transmission ratio when the carriage position changes, which could be due to the coupling between the components of this mode.

Finally, the third mode presents very low variation respect to mass changes for both transmission ratios, as Table 6 shows, due to its highly torsional predominance. However, it presents considerable variation for different carriage positions.

Table 6 Third natural frequency variation for different operating conditions

Operation conditions	$l = 10$ mm/rev (%)	$l = 32$ mm/rev (%)
Variable position	18.0	22.0
Variable mass	0.02	0.0
Variable position and mass	19.0	23.0

6 Analysis of results

The first vibration mode is predominantly axial for both transmission ratios, with a strong displacement on the carriage position, as is noticed by the large value of $\phi_{u_c 1}$ in Figs. 3a and 4a. Consequently, it presents a strong frequency shift for different operating conditions involving load mass variations, large carriage displacements, or combination of both, specially for low transmission ratios. This mode will have a strong influence on the achievable bandwidth if the control loop is closed with the direct carriage position [13]. In this case, adaptive control strategies must be used to achieve a high bandwidth closed loop [4, 10]. For this kind of control, a high transmission ratio may be preferred because the natural frequency value will be less sensitive to load mass variations.

The second mode presents low sensitivity to load mass variation for both transmission ratios and just a slight frequency shift for high transmission ratios when the carriage position changes. Therefore, a low screw lead may be preferred if the loop is closed with a rotary encoder on the motor side. In this case, just a conventional notch filter can be used to mitigate its negative effect. In addition, with a low screw lead, the first mode will be slightly reflected on the encoder signal, as is indicated by the lower value of its angular components $\phi_{\theta_{\mathrm{m}} 1}$ in Fig. 3 with respect to the corresponding one in Fig. 4.

The third mode presents a considerable frequency shift for different carriage positions but low sensitivity to mass changes. Therefore, if the application involves short carriage displacement, a notch filter can also be used when the loop is closed with a rotary encoder. Furthermore, as this mode has a relatively high frequency, it is expected to be slightly excited by typical position commands or external perturbations.

On the other hand, the knowledge of the system behavior in each mode can be very useful for identification purposes, especially at high frequencies. A convenient point to perform measurements to identify the first mode is the direct carriage position, where the largest deformation of this mode takes place, as can be seen in Fig. 3. Similarly, the angular position at the end of the screw $\theta_{x=L}$ can be a suitable point of measurement to identify the second and third modes.

7 Conclusions

A finite dimensional model of a ball screw feed-drive system is presented, where Ritz series are used to approximate the continuous field displacements of the

ball screw subsystem. This model is used to predict the behavior of the first three vibration mode shapes and their frequencies. The predominance of deformation, torsional or axial, of each mode was studied for different transmission ratios. Furthermore, the mode frequency shift for different carriage positions and load mass was studied for these modes.

Based on this analysis, the first mode is mainly axial, with a strong displacement of carriage position, whereas the second and third modes are mainly torsional. However, as the screw lead increases, the axial–torsional coupling increases accordingly and it is not suitable to consider each mode as pure axial or torsional. As the axial–torsional coupling varies, the frequency sensitivity of each mode to operating conditions varies. A strong axial–torsional coupling makes the frequency value of the first mode to be less sensitive to load mass variations. However, a low axial–torsional coupling may be preferred to minimize frequency variations of the second mode for variable carriage positions.

The transmission ratio is a key design parameter with direct influence on the degree of axial–torsional coupling, which dominates the modes frequency shift. Therefore, it has a significant effect on the robustness of the control strategies used for position control.

References

1. Hecker RL, Flores GM, Xie Q, Haran RA (2008) A review of machine-tools servocontrol level. Lat Am Appl Res (Int J) 38(1):85–94
2. Smith DA (1999) Wide bandwidth control of high-speed milling machine of feed drives. PhD dissertation, University of Florida
3. Varanasi KK, Nayfeh SA (2004) The dynamics of lead-screw drives: low-order modeling and experiments. J Dyn Syst Meas Control (ASME) 126:388–396
4. Kamalzadeh A, Erkorkmaz K (2007) Compensation of axial vibrations in ball screw drives. Ann CIRP 56(1):373–378
5. Okwudire CE, Altintas Y (2009) Minimum tracking error control of flexible ball screw drives using a discrete-time sliding mode controller. J Dyn Syst Meas Control (ASME) 131:051006
6. Erkorkmaz K, Kamalzadeh A (2006) High bandwidth control of ball screw drives. Ann CIRP 55(1):393–398
7. Altintas Y, Brecher C, Weck M, Witt S (2005) Virtual machine tool. Ann CIRP 54(2):115–138
8. Chen JS, Huang YK, Cheng CC (2004) Mechanical model and contouring analysis of high-speed ball-screw drive systems with compliance effect. Int J Adv Manuf Technol 24:241–250
9. Zaeh MF, Oertli T, Milberg J (2004) Finite element modeling of ball screw feed drive systems. Ann CIRP 53(1):289–294
10. Okwudire CE, Altintas Y (2009) Hybrid modeling of ball screw drives with coupled axial, torsional, and lateral dynamics. J Mech Des (ASME) 13(7):071002
11. Ginsberg JH (2001) Mechanical and structural vibrations theory and applications. Wiley, New York
12. Wei Ch Ch, Lin JF (2003) Kinematic analysis of the ball screw mechanism considering variable contact angles and elastic deformation. J Mech Des 125:717–733
13. Varanasi KK (2002) On the design of a precision machine for closed-loop performance. MS thesis, Massachusetts Institute of Technology, Cambridge, MA
14. Vicente DA, Hecker RL, Flores G (2007) Dynamic modeling of lead screw drives using Ritz series. In: XII RPIC, Río Gallegos, Santa Cruz, Argentina
15. Vicente DA, Hecker RL, Flores G (2008) Vibration modes characterization in a lead screw drive. In: Proceedings of MUSME, the international symposium on multibody systems and mechatronics, San Juan, Argentina, Paper n. 23-MUSME08